scientific reports

Check for updates

OPEN

Pd immobilization biguanidine modified Zr-UiO-66 MOF as a reusable heterogeneous catalyst in Suzuki–Miyaura coupling

Hojat Veisi[1]✉, Mozhdeh Abrifam[1], Sheida Ahany Kamangar[1], Mozhgan Pirhayati[2], Shokoufeh Ghahri Saremi[1], Mohammad Noroozi[3], Taiebeh Tamoradi[4]✉ & Bikash Karmakar[5]✉

In recent days, nanohybrid metal organic frameworks (MOF) have been considered as next generation catalysts due to their unique features like large surface to volume ratio, tailorable geometry, uniform pore sizes and homogeneous distribution of active sites. In this report, we address the biguanidine modified 3D Zr-centred MOF UiO-66-NH_2 following a post synthetic modification approach. Utilizing the excellent chelating ability of biguanidine, Pd ions are immobilized over the host matrix MOF. The as-synthesized material was physicochemically characterized using a broad range of analytical techniques like FT-IR, electron microscopy, EDS, elemental mapping, XRD and ICP-OES. Subsequently the material has been catalytically employed in the classical Suzuki–Miyaura coupling towards the synthesis of diverse biphenyl derivatives at sustainable conditions. There are very few reports on the covalently modified MOFs towards the organic coupling reactions. The catalyst has been isolated by centrifugation and recycled in 9 consecutive runs with almost insignificant leaching and minute decrease in reactivity.

In the recent past, scientists have witnessed unprecedented progress in catalysis, particularly after the inception and involvement of designed and engineered nanomaterials, in view of economic and environmental reasons[1–3]. With time heterogeneous catalysts have been further bejeweled when MOFs came into prominence. MOFs are porous crystalline coordination polymers (PCCP) with well-defined pore surfaces having metal nodes, being connected to organic ligands like aromatic polycarboxylates or nitrogenous heterocycles[4,5]. They acquire exceptionally large surface to volume ratio, adjustable pore dimensions, defined crystal environment, homogeneously dispersed catalytic sites throughout the matrix, tunable metal concentration and accessible to varied chemical modifications[7–10]. One of the key features of MOFs is the opportunity to architect them by selecting suitable ligand of proper size and geometry, different type of metal nodes with variable coordinating fashions that makes the pore dimensions, geometry and rigidity of the corresponding MOF absolutely predictable[11,12]. Due to such kind of exclusive features and advantages, MOF derivatives have been widely applied in gas adsorption, storage and separation, luminescence, water treatment, sensing, proton conductivity, magnetics, energy related applications, drug delivery specifically in cancer therapy, and as nano-reactor in heterogeneous catalysis[13–17]. However, questions have been raised regarding the limitation in MOFs, particularly about their physical and thermal stability[6]. In consequences to that, dealing with heterogeneous catalytic support, we selected UiO-66-NH_2, a Zr-terephthalate derived MOF, which bears significant chemical, thermal and mechanical stability as well as suitable towards post-functionalizations. The UiO-66 skeleton is constructed with $[Zr_6O_4(OH)_4]$ octahedral secondary building units (SBU) and 1,4-benzene dicarboxylate (BDC) derivatives. In bond connectivity, Zr_6 cluster is coordinated to BDC in 1:12 unit ratio three dimensionally thus affording a hierarchical framework[18–21]. There

[1]Department of Chemistry, Payame Noor University, Tehran, Iran. [2]Department of Applied Chemistry, Faculty of Science, Malayer University, Malayer, Iran. [3]Center for Research and Development of Petroleum Technologies at Kermanshah, Research Institute of Petroleum Industry (RIPI), Tehran, Iran. [4]Department of Chemistry, Production Technology Research Institute-ACECR, Ahvaz, Iran. [5]Department of Chemistry, Gobardanga Hindu College, 24-Parganas (North), Gobardanga, India. ✉email: hojatveisi@yahoo.com; t.tabss@yahoo.com; bkarmakar@ghcollege.ac.in

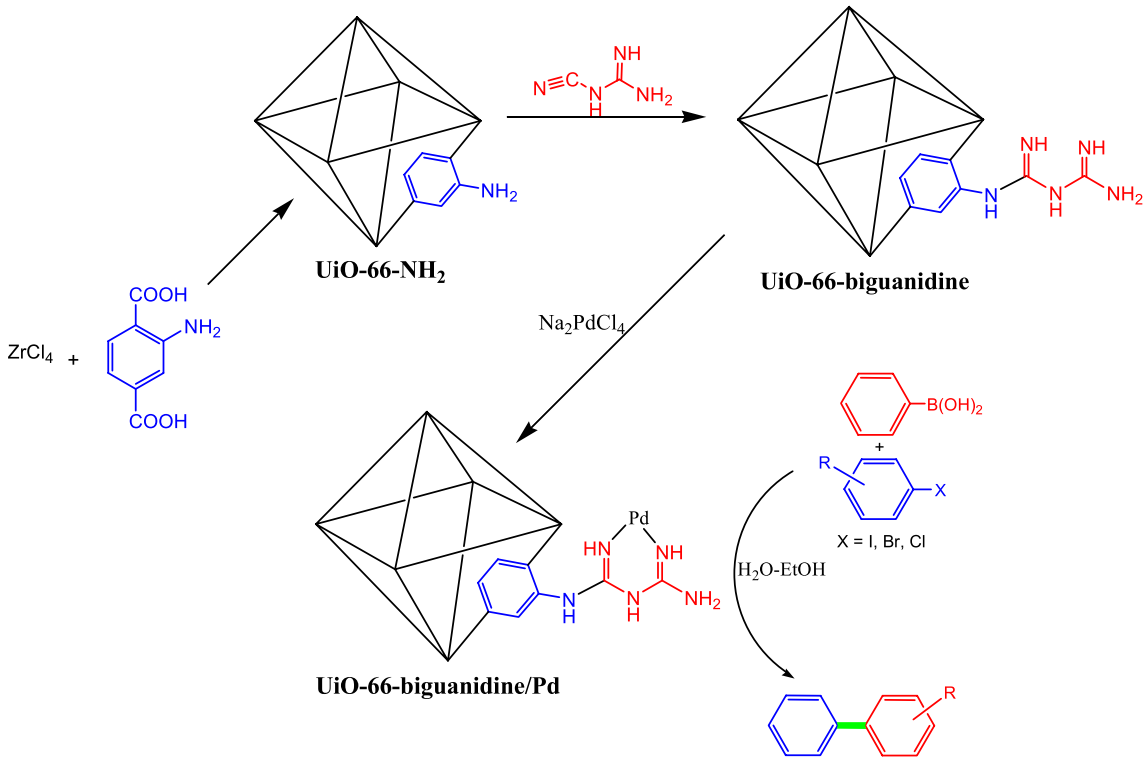

Figure 1. Sequential synthesis of UiO-66-biguanidine/Pd nanocomposite catalyst towards the Suzuki–Miyaura coupling reactions.

are several reports on the synthesis and catalytic applications of various MOF derivatives being synthesized from pre-modified ligands and post-immobilized metal ions or metal nanoparticles thereon[22–29]. However, synthetic organic applications of active metal adorned post-functionalized MOFs, has not been much explored and there are ample scopes to develop this area[30–34]. This has persuaded us to design the Zr-UiO-66 MOF using 2-amino-1,4-dicarboxylic acid ligand and subsequently covalent functionalization with cyano guanidine to generate a biguanidine moiety in situ. Biguanidine is a recognized and excellent chelating ligand and we exploited it to anchor Pd ions at the outer-shell of Zr-UiO-66-NH_2.

In synthetic organic chemistry carbon–carbon bond formation is measured as one of the most fundamental and challenging reactions[35–37]. Among the several such categories, Suzuki–Miyaura coupling is considered as a protagonist and used in the synthesis of diverse symmetric and asymmetric biphenyl compounds which have otherwise applications as important hypertensive, antimicrobial, fungicide, anti-diabetic and analgesic drugs[38–43]. There are prolific reports on the Suzuki–Miyaura coupling methodology over different Pd catalysts[44–49]. However, the Pd functionalized biguanidine modified Zr-UiO-66 MOF (Fig. 1) on the Suzuki coupling is not reported so far. Hence, we introduce a green and competent protocol on the Suzuki reaction by coupling a wide range of aryl halides with phenylboronic acid over UiO-66-biguanidine/Pd nanocomposite. Operational simplicity, green reaction conditions, simple and inexpensive procedure, high efficiency, short reaction times, easy separation of the catalyst and reusability for several consecutive cycles are the key advantages of this protocol.

Experimental

Preparation of UiO-66-biguanidine. UiO-66-biguanidine is synthesized as our previous report[50].

Preparation of UiO-66-biguanidine/Pd. A uniformly dispersed solution of UiO-66-biguanidine was prepared by sonication in 50 mL H_2O which was followed by addition an aqueous solution of Na_2PdCl_4 (15 mL, 2 mg mL^{-1}) as Pd precursor and stirred for 12 h. The resulting solid was collected by centrifuge, washed twice with 20 mL DI water and then with 20 mL ethanol. Finally, the UiO-66-biguanidine/Pd was dried in vacuum at 60 °C for 24 h. The Pd load in the material was found 0.18 mmol/g, being estimated via ICP-OES method.

Suzuki–Miyaura coupling over UiO-66-biguanidine/Pd nanocomposite catalyst. A mixture of Aryl halide, phenyl boronic acid and K_2CO_3 in 1:1:2 molar ratio was stirred in aqueous EtOH (3 mL) and then the catalyst (30 mg, 0.1 mol %) was added and gently warmed at 50 °C for proposed time. After completion (by TLC), EtOAc was added to the mixture and the catalyst was isolated off. The entire mixture was soaked over anhydrous Na_2SO_4 and the organic layer obtained was evaporated to get the biphenyl product in almost pure form. They were further purified by passing over a silica gel (100–200 mesh) filter column with 5% EtOAc/Hexane as eluent.

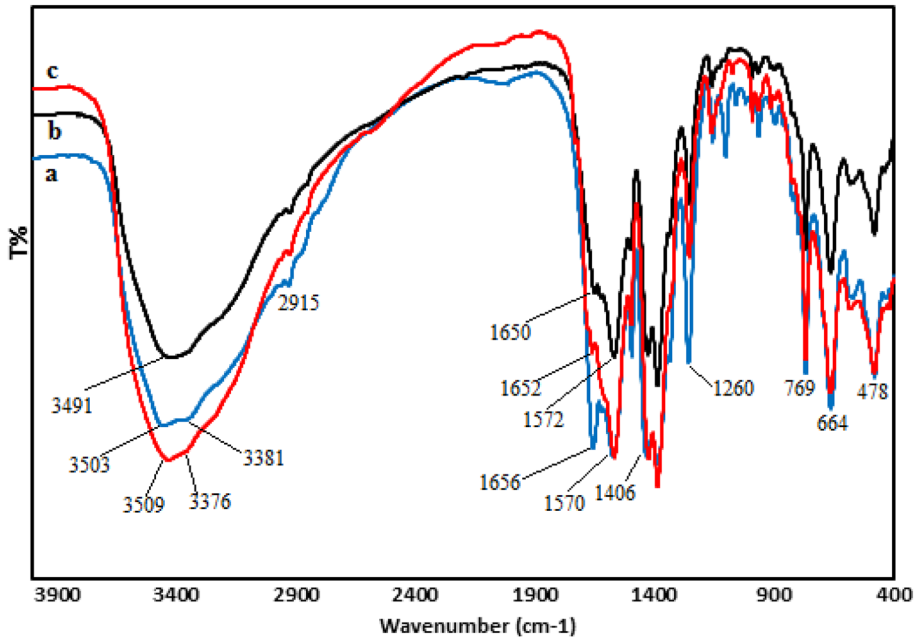

Figure 2. FT-IR spectra of UiO-66-NH_2 (**a**), UiO-66-biguanidine (**b**) and UiO-66-biguanidine/Pd (**c**).

Results and discussions

Catalyst characterization data analysis. Physicochemical characteristics of the as synthesized catalyst were determined following a detailed analysis over FT-IR, SEM, EDX, elemental mapping, TEM and XRD study. A comparative FT-IR analysis between UiO-66-NH_2, UiO-66-biguanidine and UiO-66-biguanidine/Pd materials have been showed in Fig. 2. The bare UiO-66-NH_2 can be identified by the characteristic vibrations at 1406 and 1570 cm^{-1}, attributed to the symmetric and asymmetric stretching of COOH groups from BDC (Fig. 2a). Amino function can be detected by the H–N–H scissoring, C-NH_2 stretching, N–H symmetric and asymmetric stretching vibrations at 1260 cm^{-1}, 1656 cm^{-1}, 3381 cm^{-1} and 3503 cm^{-1} respectively[20,26]. In the synthesis of UiO-66-biguanidine, the UiO-66-NH_2 reacts with cyano guanidine and the change in bonding can be evidenced from FT-IR spectrum. In Fig. 2b, representing the UiO-66-biguanidine, the two N–H stretching peaks are disappeared while the other peaks remained almost unaltered, as the free amine is replaced by guanidine scaffold[50]. Though, no considerable differences being detected between the spectrum of Fig. 2b from Fig. 2c, except a sight shifting of peaks at lower region due to the strong coordination of Pd nanoparticles to the biguanidine ligand (Fig. 2c).

The particle size, shape, dimensions and textural morphology was investigated over SEM. Figure 3 depicts the particle images at different magnifications. The nanocrystals are homomorphic and cubical in shape with an average dimension of 40 to 80 nm. The Pd association or surface functionalization leaves no significant changes in the apparent morphology. The particles seem to be somewhat agglomerated due to high concentration during sampling.

The elemental composition of UiO-66-NH_2 and the final material was ascertained by EDX analysis as shown in Fig. 4. The profile of UiO-66-NH_2 displays the signals of Zr, N and O atoms, indicating Zr and N, O species being contributed from as SBU and BDC respectively (Fig. 4a). Figure 4b demonstrates the profile of UiO-66-biguanidine/Pd, presenting the same elements along with Pd and C. C species correspond to the attached organic ligand (biguanidine) and Pd being immobilized over it.

Additionally, surface allocation of the corresponding elements in UiO-66-biguanidine/Pd was ascertained by the X-ray elemental mapping study. A segment of the SEM image of the catalyst was scanned by X-ray and the outcome is displayed in Fig. 5. It evidently shows the homogeneous dispersion of Zr, C, O, N and Pd. Obviously, Zr is having much higher density than Pd as the former is the basic constructive unit of the material. Again, the dispersed Pd is observed to be of higher concentration than N. This can be corroborated as Pd is not only bonded to the guanidine moiety, but also associated inside the MOF structure. Nevertheless, the uniform distribution of Pd has significant importance behind its outstanding catalytic activity.

The TEM images of UiO-66-NH_2 and UiO-66-biguanidine/Pd materials are presented in Fig. 6. As the Fig. 6a,b shows, UiO-66-NH_2 represent a poorly crystalline discrete structure. However, in the final material the Pd NPs are clearly can be observed as round shaped black dots spread over the UiO-66-biguanidine MOF support. The monodispersed NPs have an average diameter of 20 nm (Fig. 6c,d).

XRD study were carried out to investigate the phase and crystalline morphology of UiO-66-NH_2 and UiO-66-biguanidine/Pd, being depicted in Fig. 7. Evidently, both the materials have poor crystallinity, as predicted from TEM image. XRD profile of UiO-66-NH_2 represents three characteristic diffraction peaks appeared at $2\theta = 7.3$, 8.7 and 26.1° respectively, being comparable to previous literature[51]. Apparently, both the materials exhibit roughly similar XRD patterns, signifying conservation of internal framework upon post-synthetic modifications. However, no significant peaks were detected due to the attached Pd species.

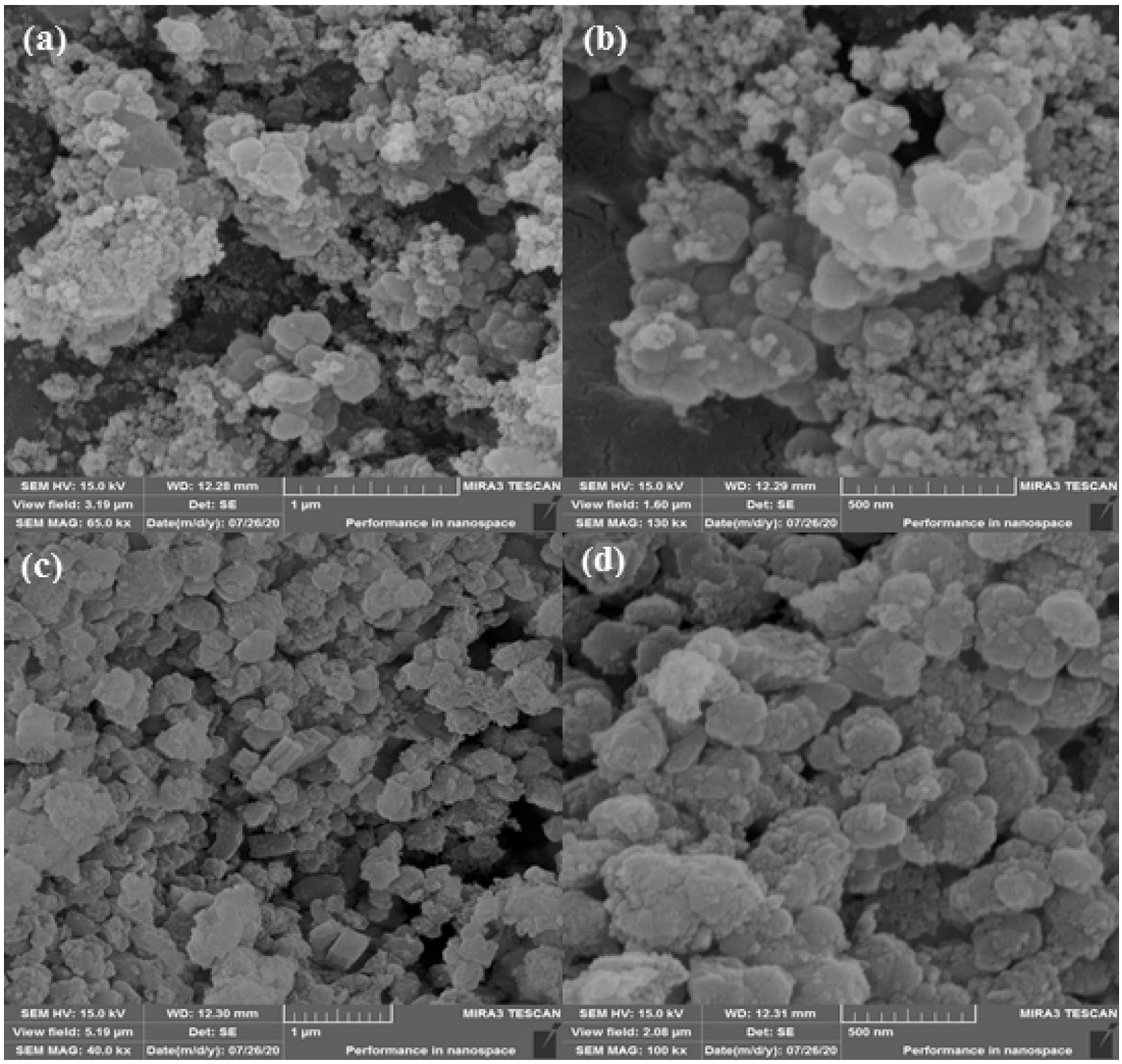

Figure 3. SEM images of UiO-66-NH_2 (**a**,**b**); and UiO-66-biguanidine/Pd nanocomposite (**c**,**d**).

Surface analysis of UiO-66-biguanidine and UiO-66-biguanidine/Pd materials were investigated through nitrogen adsorption–desorption study and the corresponding outcomes have been presented in Table 1. Langmuir surface area of the two materials were found 831 and 629 m^2/g respectively. The lower surface area of the latter can be anticipated due to immobilization of Pd nanoparticles and partially blocking the pores lying on the surface of MOF. This is the reason for its reduced pore volume and pore diameter as compared to its precursor. Langmuir isotherm of UiO-66-biguanidine/Pd has been shown in Fig. 8, which is a typical type I isotherm indicating the material to be microporous in nature.

On having scrupulous catalytic characterizations and analyses, it was the time for catalytic explorations and the effect was studied in Suzuki–Miyaura reaction following a straightforward pathway. On completion, the catalyst was isolated by centrifuge for further runs. Nevertheless, with the aim of having the standardized conditions, a probe reaction between phenyl boronic acid and 4-boromotoluene was set to notice the effect of variable conditions like solvent, applied base, Pd load and temperature and the results are documented in Table 2. The investigations were started with 0.1 mol% Pd loaded catalyst and K_2CO_3 as base (2.0 mmol). When we investigated the probe in diverse solvents like DMF, toluene, EtOH and H_2O, the optimum result was obtained in aqueous EtOH (1:1) (Table 3, entries 1–5). On the other hand, while carrying out the reaction in the absence of base, a weak productivity was encountered, implying its significance (Table 4, entry 4). Thereby, we investigated the effect of various bases like Et_3N, Na_2CO_3 and K_2CO_3, when the last one afforded the highest yield (Table 4, entries 1–3). Among the different Pd loaded catalysts, we found the 0.1 mol% worked as the optimum (Table 5, entries 1–3). There was no product at all over the Pd free bare catalyst (Table 5, entry 4). Finally, we also studied the effect of temperature keeping the best solvent, catalyst and base. From Table 6 it is evident that the reaction does not produce satisfactory yields at lower temperatures like 25 °C and 40 °C (entry 2,4) and optimum result was obtained at 50 °C (entry 1).

After having the optimized conditions, we wished to investigate their generalizations and scope. Diverse array of biaryls were synthesized by coupling various haloarenes and phenylboronic acid following the stabilized conditions (Table 7). In the entire scenario, the chlorobenzenes were found to react sluggishly as compared to bromo

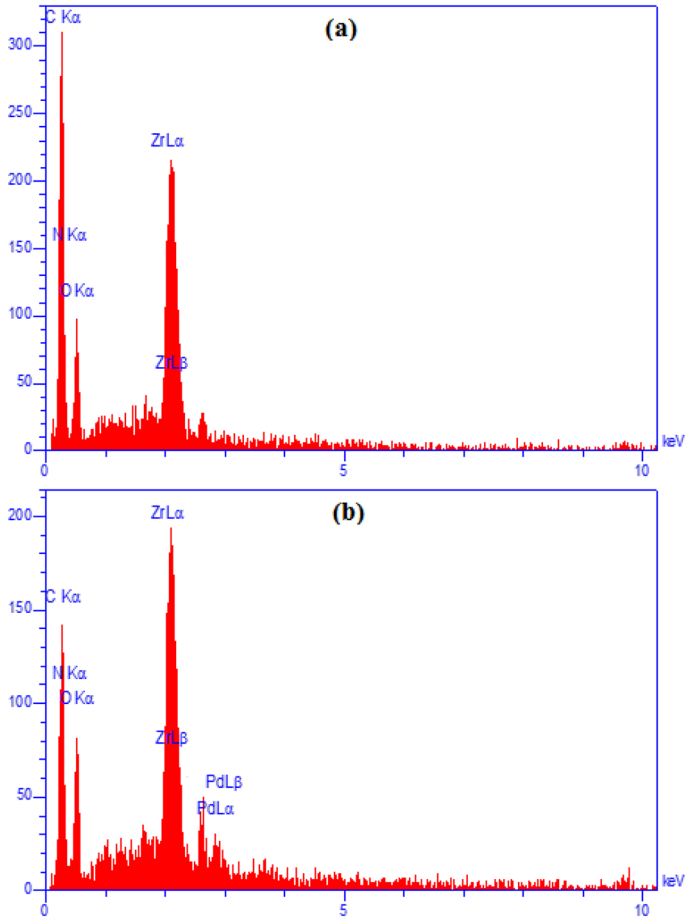

Figure 4. EDX spectra of UiO-66-NH_2 (**a**); and UiO-66-biguanidine/Pd nanocomposite (**b**).

or iodoarenes which is manifested from their yields and reaction times. A wide variety of bromo and iodoarenes having electron withdrawing ($COCH_3$) or electron donating substituent (CH_3, OCH_3, NH_2, OH) were found very well compatible under the optimized conditions. Markedly, we achieved very good productivity with heteroaryl halides like 2-bromothiophene and 2-iodothiophene as substrate (Table 7, entries 16–17) coupled fruitfully with high yields. All the reactions were completed within 10–60 min except those with chloroarenes which were mostly sluggish. This can be explained based on strong electronegativity and the poor leaving capacity of Cl atom.

Reusability study of catalyst. In consideration of heterogeneous green catalysis, an exploration of recyclability of the corresponding catalyst seems a crucial principle. On completion of a fresh batch of probe, it was isolated by centrifuge and rinsed thoroughly with aqueous EtOH. Subsequently, it was dried and reused in the further cycles. The UiO-66-biguanidine/Pd nanocomposite displayed significant activity up to 7 successive cycles without considerable reduction in reactivity. However, the yield fell down to 90% and 86% in 8th and 9th cycle (Fig. 9). This could be due to aerial oxidation of active species, agglomeration of Pd NPs or deposition of organic species over them. We further analyzed the structural morphology of UiO-66-biguanidine/Pd catalyst after recycling 9 times by using XRD and FT-IR. The results shown that the catalyst retains its initial morphology and structure without any change (Fig. 10), which in turn validates the robustness of our material.

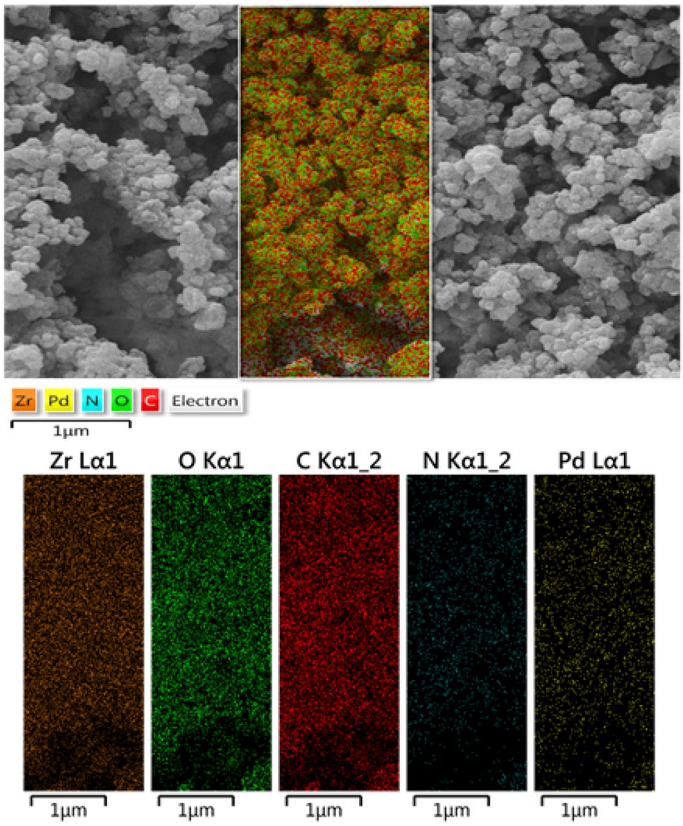

Figure 5. Elemental mapping of nanocomposite UiO-66-biguanidine/Pd with the atomic distribution of Zr, O, C, N, and Pd.

Uniqueness of our results. To ascertain the distinctiveness of our devised catalytic system, a systematic comparison with a number of other protocols in the coupling between phenylboronic acid and bromo and iodooarenes has been done. Evidently, the UiO-66-biguanidine/Pd nanocomposite reveals a superior result in terms of TOF, as shown in Table 8.

Conclusion

In summary, we introduce a biguanidine modified Zr-UiO-66 metal organic framework with Pd NPs being decorated over its surface. Pd NPs were immobilized following a post-functionalization of biguanidine over the core UiO-66-NH_2 MOF than the typical surface deposition. The excellent chelating potential of biguanidine was exploited to deposit Pd NPs over it. Structural morphology and physicochemical features of the material were explored over different instrumental methods. Atomic mapping analysis displays the uniform dispersion of active sites throughout the surface matrix. The nanocatalyst has been deployed in the C–C coupling via Suzuki–Miyaura reactions under mild and green conditions to synthesize a wide variety of biphenyl derivatives affording outstanding yields. The robustness of the material has been validated by recycling it for 9 consecutive cycles without momentous loss of its reactivity. There is also negligible leaching of Pd species in the reaction medium, justifying its true heterogeneity.

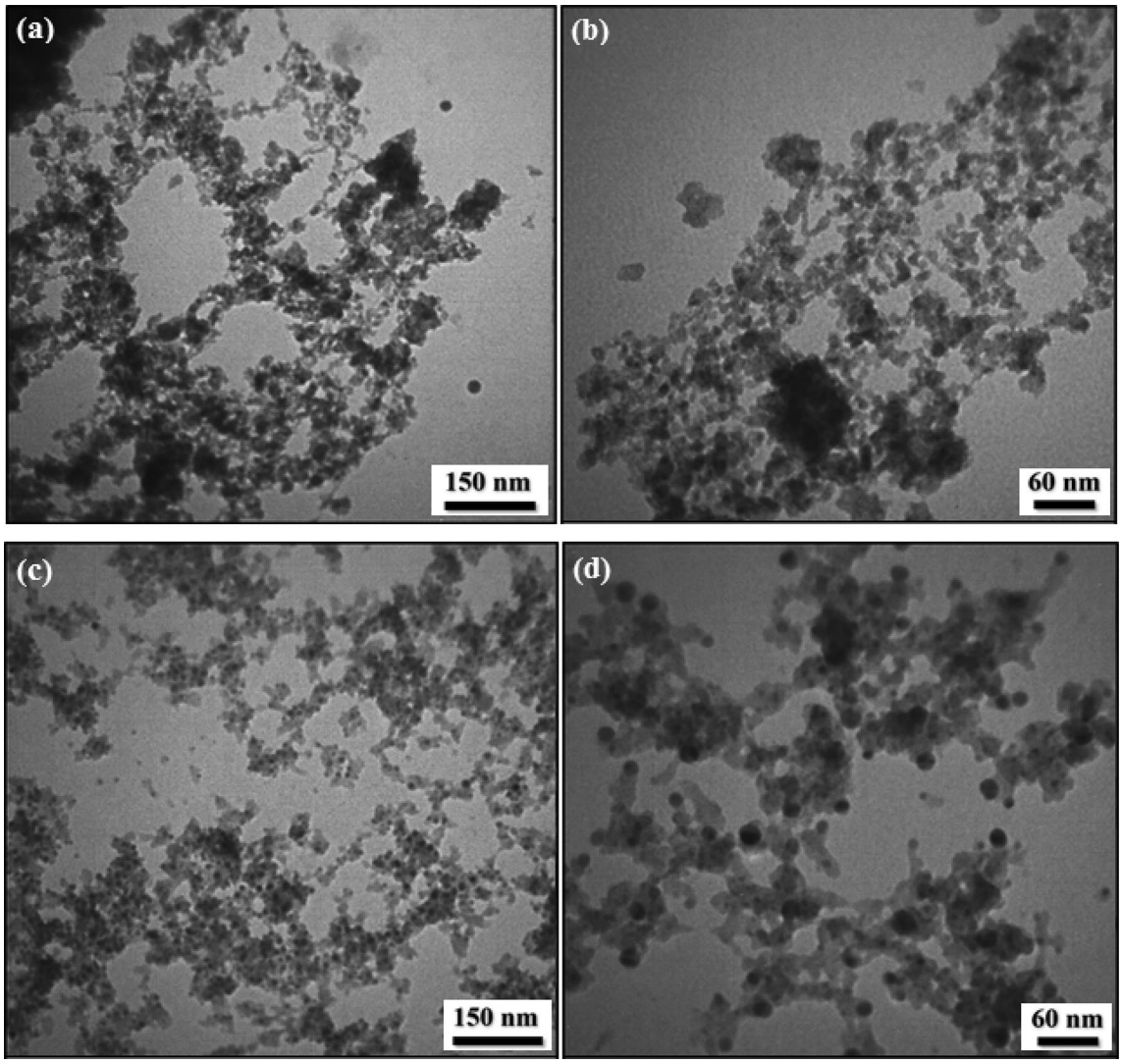

Figure 6. TEM images of UiO-66-NH_2 (**a**,**b**); and UiO-66-biguanidine/Pd nanocomposite (**c**,**d**).

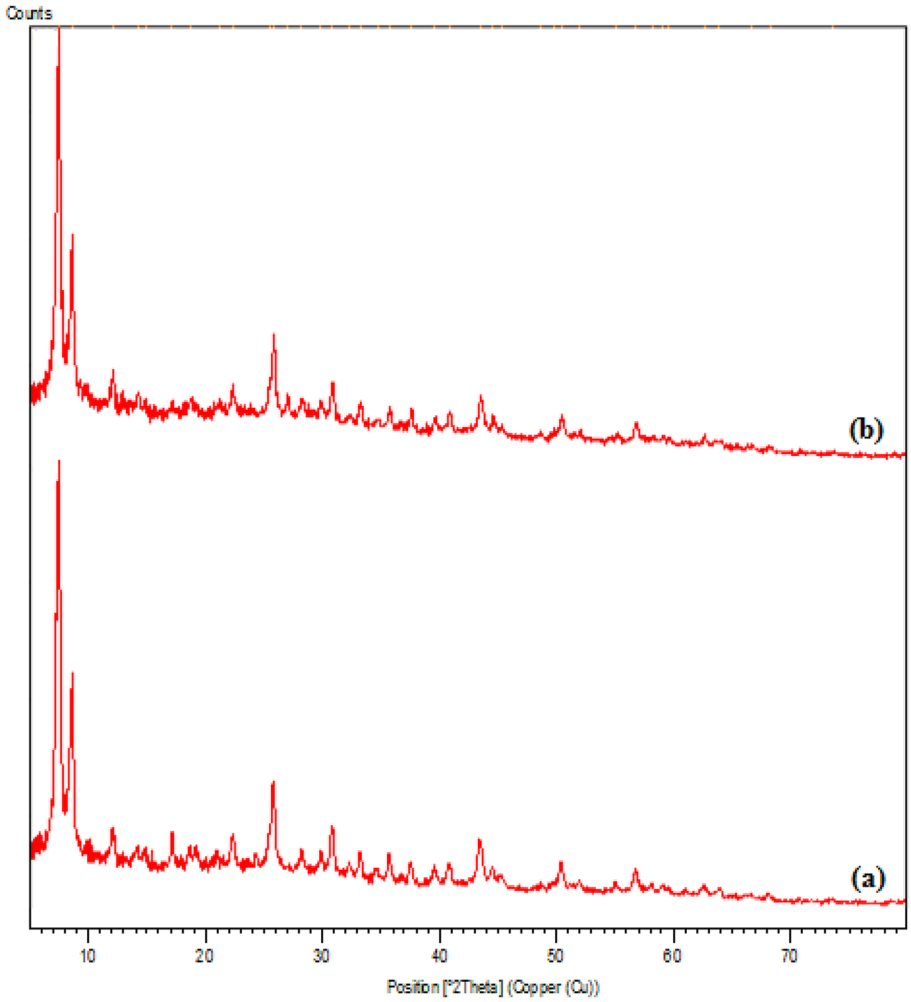

Figure 7. XRD patterns of UiO-66-NH_2 (**a**); and UiO-66-biguanidine/Pd (**b**).

Entry	Samples	S_{BET} (m^2g^{-1})	Total pore volume (cm^3g^{-1})	Mean pore diameter (nm)
1	UiO-66-biguanidine	831	0.52	0.58
2	UiO-66-biguanidine/Pd	629	0.41	0.51

Table 1. Nitrogen adsorption–desorption data for UiO-66-biguanidine and UiO-66-biguanidine/Pd.

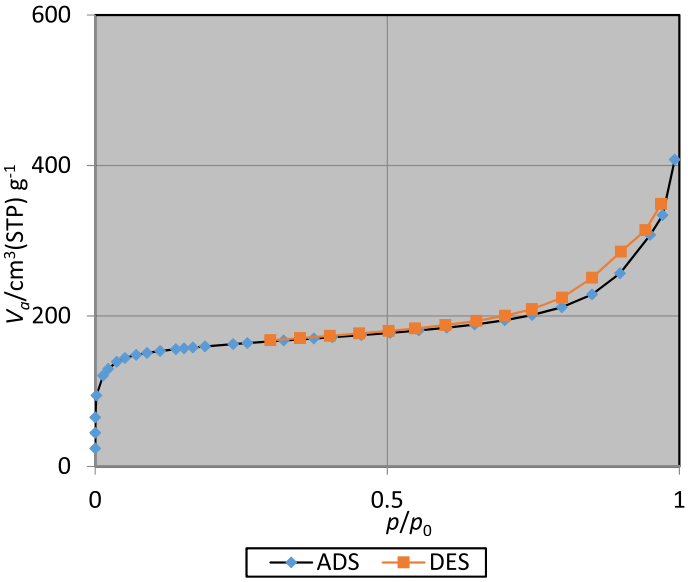

Figure 8. N_2-adsorption isotherms of UiO-66-biguanidine/Pd.

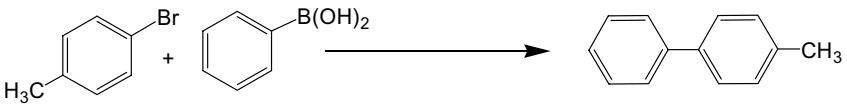

Table 2. The optimization study in the reaction of 4-bromotoluene with phenyl boronic acid over UiO-66-biguanidine/Pd[a].

Entry	Solvent	Time (Min)	Yield (%)
1	DMF	60	65
2	Toluene	60	55
3	EtOH	60	70
4	H_2O	120	50
5	**EtOH/H_2O (1:1)**	**20**	**96**

Table 3. Screening of solvent. Reaction conditions: 4-methylbromobenzene (1.0 mmol), phenylboronic acid (1.0 mmol), UiO-66-biguanidine/Pd, K_2CO_3 as base (2 mmol) and solvent (3 mL) at 50 °C; Isolated yield.

Entry	Base	Time (Min)	Yield (%)
1	**K_2CO_3**	**20**	**96**
2	Et_3N	60	60
3	Na_2CO_3	60	70
4	No base	120	Trace

Table 4. Screening of base. Reaction conditions: 4-methylbromobenzene (1.0 mmol), phenylboronic acid (1.0 mmol), UiO-66-biguanidine/Pd, EtOH/H_2O (1:1) as solvent (3 mL) at 50 °C; Isolated yield.

Entry	Pd (mol%)	Time (Min)	Yield (%)
1	**0.1**	**20**	**96**
2	0.05	30	70
3	0.2	20	96
4	0.0	120	0

Table 5. Variation of catalyst load. Reaction conditions: 4-methylbromobenzene (1.0 mmol), phenylboronic acid (1.0 mmol), K_2CO_3 as base (2 mmol), EtOH/H_2O (1:1) as solvent (3 mL) at 50 °C; Isolated yield.

Entry	T (°C)	Time (Min)	Yield (%)
1	**50**	**20**	**96**
2	25	120	75
3	60	20	96
4	40	30	70

Table 6. Variation of temperature. Reaction conditions: 4-methylbromobenzene (1.0 mmol), phenylboronic acid (1.0 mmol), UiO-66-biguanidine/Pd (0.1 mol% Pd), K_2CO_3 as base (2 mmol), EtOH/H_2O (1:1) as solvent (3 mL); Isolated yield.

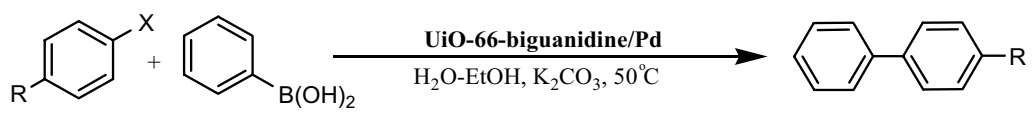

Entry	RC_6H_4X	X	Time (min)	Yield (%)[b]
1	H	I	10	98
2	H	Br	15	98
3	H	Cl	120	50
4	4-CH_3	I	10	96
5	4-CH_3	Br	20	96
6	4-CH_3	Cl	120	45
7	4-$COCH_3$	I	20	96
8	4-$COCH_3$	Br	45	96
9	4-$COCH_3$	Cl	120	40
10	4-CH_3O	I	30	96
11	4-CH_3O	Br	45	90
12	4-NH_2	I	45	90
13	4-NH_2	Br	90	82
14	4-OH	I	60	90
15	4-OH	Br	120	85
16	2-Thienyl	I	60	92
17	2-Thienyl	Br	120	88

Table 7. Catalytic activity of UiO-66-biguanidine/Pd nanocomposite in Suzuki–Miyaura coupling reactions. [a]Reaction conditions: 1.0 mmol arylhalide,1.0 mmol phenylboronic acid, 2 mmol K_2CO_3, 0.03 g catalyst (0.1 mol% Pd), 3 mL of H_2O/EtOH (1:1), 50 °C, [b]Isolated yield.

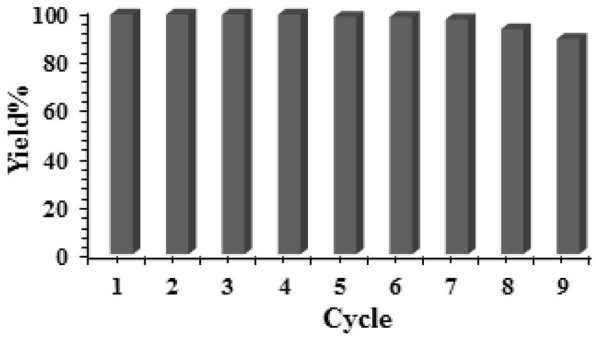

Figure 9. The recycling of the UiO-66-biguanidine/Pd nanocomposite.

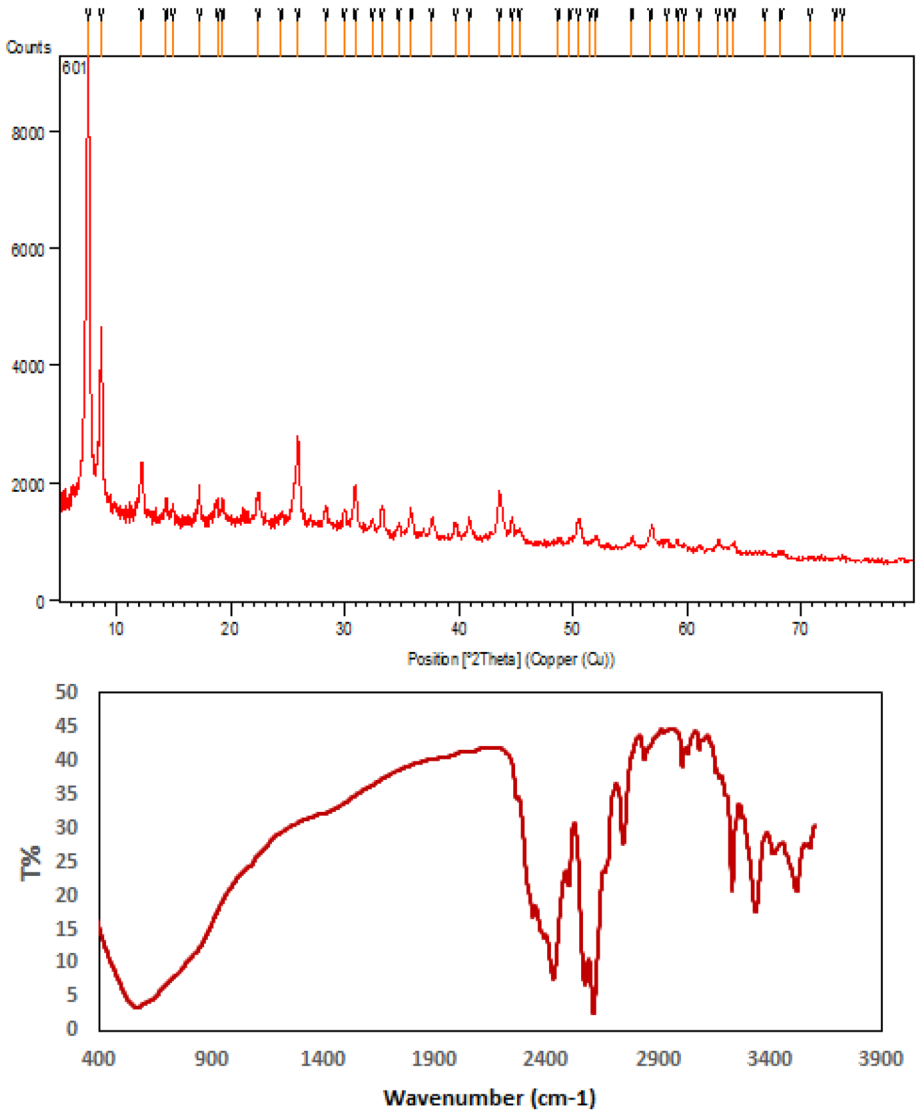

Figure 10. XRD and FT-IR data for reused UiO-66-biguanidine/Pd catalyst after 9 runs.

Entry	Catalyst (mol%)	Conditions	X	TOF (h^{-1})[a]	Refs
1	Bis(oxamato)palladate(II) complex (5)	Et_3N, *n*-Bu_4NBr, 120 °C	I, Br	7.8, 6.5	[52]
2	NHC-Pd(II) complex (0.2)	$K_3PO_4.3H_2O$, H_2O, TBAB, 40 °C	I, Br	98, 75	[53]
3	SiO_2-pA-Cyan-Cys-Pd (0.5)	K_2CO_3, H_2O, 100 °C	I, Br	38, 32	[54]
4	Pd_3(dba) (1)	K_3PO_4, THF, 80 °C	Br	3.2	[55]
5	Pd–BOX (2)	K_2CO_3, DMF, 70 °C	I	8.3	[56]
6	γ -Fe_2O_3-acetamidine-Pd (0.12)	Et_3N, DMF, 100 °C	I, Br	1600, 1600	[57]
7	Pd-isatin Schiff base-γ-Fe_2O_3 (0.5, 1.5)	Et_3N, Solvent-free, 100 °C	I, Br	380, 85.7	[58]
8	UiO-66-biguanidine/Pd (0.1)	K_2CO_3, H_2O-EtOH, 50 °C	I, Br	11,870, 3920	this work

Table 8. Catalytic Comparison in the reaction between phenyl boronic acid and iodobenzene. [a]TOF, turnover frequencies (TOF = (Yield/Time)/Amount of catalyst (mol).

Received: 22 March 2021; Accepted: 14 October 2021
Published online: 08 November 2021

References

1. Astruc, D. Introduction: Nanoparticles in catalysis. *Chem. Rev.* **120**(2), 461–463 (2020).
2. Liu, L. & Corma, A. Metal catalysts for heterogeneous catalysis: From single atoms to nanoclusters and nanoparticles. *Chem. Rev.* **118**, 4981–5079 (2018).
3. Rodrigues, T. S., da Silva, A. G. M. & Camargo, P. H. C. Nanocatalysis by noble metal nanoparticles: Controlled synthesis for the optimization and understanding of activities. *J. Mater. Chem. A* **7**, 5857–5874 (2019).
4. Dhakshinamoorthy, A., Santiago-Portillo, A., Asiri, A. M. & Garcia, H. *ChemCatChem* **11**, 899–923 (2019).
5. Liu, J. *et al. Chem. Soc. Rev.* **43**, 6011–6061 (2014).
6. Gascon, J., Corma, A., Kapteijn, F. & Llabre, F. X. Metal organic framework catalysis: Quo vadis?. *ACS Catal.* **4**, 361–378 (2014).
7. Dhakshinamoorthy, A., Opanasenko, M., Cejka, J. & Garcia, H. Metal organic frameworks as heterogeneous catalysts for the production of fine chemicals. *Catal. Sci. Technol.* **3**, 2509–2540 (2013).
8. Dhakshinamoorthy, A., Asiri, A. M. & Garcia, H. Catalysis by metal-organic frameworks in water. *Chem. Commun.* **50**, 12800–12814 (2014).
9. Cui, W. J., Zhang, G. Y., Hu, T. L. & Bu, X. H. Metal-organic framework-based heterogeneous catalysts for the conversion of C1 chemistry: CO, CO2 and CH_4. *Coordination Chem. Rev.* **387**, 79–120 (2019).
10. Gole, B., Sanyal, U., Banerjee, R. & Mukherjee, P. S. High loading of Pd nanoparticles by interior functionalization of MOFs for heterogeneous catalysis. *Inorg. Chem.* **55**, 2345–2354 (2016).
11. Stock, N. & Biswas, S. Synthesis of metal-organic frameworks (MOFs): Routes to various MOF topologies, morphologies, and composites. *Chem. Rev.* **112**, 933–969 (2012).
12. Lu, W. *et al.* Tuning the structure and function of metalorganic frameworks via linker design. *Chem. Soc. Rev.* **43**, 5561–5593 (2014).
13. Huang, Y.-B., Liang, J., Wang, X.-S. & Cao, R. Multifunctional metal-organic framework catalysts: Synergistic catalysis and tandem reactions. *Chem. Soc. Rev.* **46**, 126–157 (2017).
14. Zhou, H. C. & Kitagawa, S. Metal-organic frameworks (MOFs). *Chem. Soc. Rev.* **43**, 5415–5418 (2014).
15. Pascanu, V., Miera, G. G., Inge, A. K. & Matute, B. M. Metal–organic frameworks as catalysts for organic synthesis: A critical perspective. *J. Am. Chem. Soc.* **141**, 7223–7234 (2019).
16. Liao, W.-M. *et al.* Tailoring exciton and excimer emission in an exfoliated ultrathin 2D metal-organic framework. *Nat. Commun.* **9**, 2401 (2018).
17. Yang, Q., Xu, Q. & Jiang, H.-L. Metal-organic frameworks meet metal nanoparticles: Synergistic effect for enhanced catalysis. *Chem. Soc. Rev.* **46**, 4774–4808 (2017).
18. Bakuru, V. R., Davis, D. & Kalidindi, S. B. Cooperative catalysis at the metal–MOF interface: Hydrodeoxygenation of vanillin over Pd nanoparticles covered with a UiO-66(Hf) MOF. *Dalton Trans.* **48**, 8573–8577 (2019).
19. Nasrabadi, M., Ghasemzadeh, M. A. & Monfared, M. R. Z. Preparation and characterization of UiO-66 metal-organic frameworks for the drug delivery of ciprofloxacin and evaluation of their antibacterial activities. *New. J. Chem.* **43**, 16033–16040 (2019).
20. Lv, H. *et al.* Enhanced synergistic antibacterial activity through a smart platform based on UiO-66 combined with photodynamic therapy and chemotherapy. *Langmuir* **36**(15), 4025–4032 (2020).
21. Chen, Y.-Z. & Jiang, H.-L. Porphyrinic metal–organic framework catalyzed heck-reaction: Fluorescence "turn-on" sensing of Cu(II) ion. *Chem. Mater.* **28**, 6698–6704 (2016).
22. Mollabagher, H., Taheri, S., Mojtahedia, M. M. & Seyedmousavib, S. A. Cu-metal organic frameworks (Cu-MOF) as an environment-friendly and economical catalyst for one pot synthesis of tacrine derivatives. *RSC Adv.* **2020**, 10 (1995).
23. Plessers, E., Fu, G., Tan, C. Y. X., de Vos, D. E. & Roeffaers, M. B. J. Zr-based MOF-808 as Meerwein–Ponndorf–Verley reduction catalyst for challenging carbonyl compounds. *Catalysts* **6**, 104–114 (2016).
24. Tambat, S. N. *et al.* Hydrothermal synthesis of NH_2-UiO-66 and its application for adsorptive removal of dye. *Adv. Powder. Technol.* **29**, 2626–2632 (2018).
25. Kandiah, M. *et al.* Post-synthetic modification of the metal–organic framework compound UiO-66. *J. Mater. Chem.* **20**, 9848–9851 (2010).
26. Chen, T. F. *et al.* Modified UiO-66 frameworks with methylthio, thiol and sulfonic acid function groups: The structure and visible-light-driven photocatalytic property study. *Appl. Catal. B: Environ.* **259**, 184047 (2019).
27. Saleem, H., Rafique, U. & Davies, R. P. Investigations on post-synthetically modified UiO-66-NH_2 for the adsorptive removal of heavy metal ions from aqueous solution. *Micropor. Mesopor. Mater.* **221**, 238–244 (2016).
28. Xiang, W., Zhang, Y., Lin, H. & Liu, C. J. Nanoparticle/metal–organic framework composites for catalytic applications: Current status and perspective. *Molecules* **22**, 2103–2126 (2017).
29. Zhu, J., Wu, L., Bu, Z., Jie, S. & Li, B. G. Polyethyleneimine-modified UiO-66-NH_2(Zr) metal-organic frameworks: Preparation and enhanced CO_2 selective adsorption. *ACS Omega* **4**, 3188–3179 (2019).

30. Luan, Y., Gao, H., Andriamitantsoa, R. S., Zheng, N. & Wang, G. A general post-synthetic modification approach of amino-tagged metal–organic frameworks to access efficient catalysts for the Knoevenagel condensation reaction. *J. Mater. Chem. A* **3**, 17320–17331 (2015).
31. Konnerth, H. *et al.* Metal-organic framework (MOF)-derived catalysts for fine chemical production. *Coord. Chem. Rev.* **416**, 213319–213342 (2020).
32. Zhu, L., Liu, X.-Q., Jiang, H.-L. & Sun, L.-B. Metal-organic frameworks for heterogeneous basic catalysis. *Chem. Rev.* **117**(12), 8129–8176 (2017).
33. Koushik, S. & Velmathi, S. Engineering metal-organic framework catalysts for C–C and C–X coupling reactions: Advances in reticular approaches from 2014–2018. *Chem. Eur. J.* **25**, 16451–16505 (2019).
34. Li, P., Regati, S., Huang, H. C., Arman, H. D. & Chen, B. L. A sulfonate-based Cu(I) metal-organic framework as a highly efficient and reusable catalyst for the synthesis of propargylamines under solvent-free conditions. *Chin. Chem. Lett.* **26**, 6–10 (2015).
35. Yin, L. & Leibscher, J. Carbon-carbon coupling reactions catalyzed by heterogeneous palladium catalysts. *Chem. Rev.* **107**, 133–173 (2007).
36. Biffis, A., Centomo, P., Zotto, A. D. & Zecca, M. Pd metal catalysts for cross-couplings and related reactions in the 21st century: a critical review. *Chem. Rev.* **118**, 2249–2295 (2018).
37. Nasrollahzadeh, M., Issaabadi, Z., Tohidi, M. M. & Sajadi, S. M. Recent progress in application of graphene supported metal nanoparticles in C–C and C–X coupling reactions. *Chem. Rec.* **18**, 165–229 (2018).
38. Mohazzab, F. B., Jaleh, B., Issaabadi, Z., Nasrollahzadeh, M. & Varma, R. S. Stainless steel mesh-GO/Pd NPs: catalytic applications of Suzuki-Miyaura and Stille, coupling reactions in eco-friendly media. *Green Chem.* **21**, 3319–3327 (2019).
39. Shen, C., Shen, H., Yang, M., Xia, C. & Zhang, P. A novel D-glucosamine-derived pyridyl-triazole@palladium catalyst for solvent-free Mizoroki-Heck reactions and its application in the synthesis of Axitinib. *Green Chem.* **17**, 225–230 (2015).
40. Negishi, E. I. Magical power of transition metals: Past, present, and future. *Angew. Chem. Int. Ed.* **50**, 6738–6764 (2011).
41. Orha, L., Tukacs, J. M., Kollár, L. L. & Mika, T. Palladium-catalyzed Sonogashira coupling reactions in γ-valerolactone-based ionic liquids. *Beilstein J. Org. Chem.* **15**, 2907–2913 (2019).
42. Bhattacharjya, A., Klumphu, P. & Lipshutz, B. H. *Nat. Commun.* **6**, 7401–7406 (2015).
43. Cherney, A. H. & Reisman, S. E. Pd-catalyzed Fukuyama cross-coupling of secondary organozinc reagents for the direct synthesis of unsymmetrical ketones. *Tetrahedron* **70**, 3259–3265 (2014).
44. Hooshmand, S. E., Heidari, B., Sedghi, R. & Varma, R. S. Recent advances in the Suzuki-Miyaura cross-coupling reaction using efficient catalysts in eco-friendly media. *Green Chem.* **21**, 381–405 (2019).
45. Duan, L. *et al.* Activation of aryl chlorides in water under phase-transfer agent-free and ligand-free Suzuki coupling by heterogeneous palladium supported on hybrid mesoporous carbon. *ACS Catal.* **5**, 575–586 (2015).
46. Veisi, H., Ozturk, T., Karmakar, B., Tamoradi, T. & Hemmati, S. In situ decorated palladium nanoparticles onto chitosan-encapsulated Fe_3O_4/SiO_2-NH_2 nanoparticles (Fe_3O_4/SiO_2-NH_2@CS/Pd NPs) as effective and recyclable catalyst in Suzuki-Miyaura coupling and 4-nitrophenol reduction. *Carbohyd. Polym.* **35**, 115966–115973 (2020).
47. Tamoradi, T., Veisi, H. & Karmakar, B. Pd Nanoparticle fabricated tetrahydroharman-3-carboxylic acid analog immobilized magnetic nanoparticle catalyzed fast and expedient C-C cross coupling Suzuki and Stille reactions and C–S coupling towards aryl thioethers. *Chem. Select* **4**, 10953–10959 (2019).
48. Hong, K. *et al.* Palladium nanoparticles on assorted nanostructured supports: Applications for Suzuki, Heck, and Sonogashira cross-coupling reactions. *ACS Appl. Nano Mater.* **3**, 2070–2103 (2020).
49. Nasrollahzadeh, M., Issaabadi, Z. & Varma, R. S. Magnetic lignosulfonate-supported Pd complex: Renewable resources-derived catalyst for aqueous Suzuki–Miyaura reaction. *ACS Omega* **4**, 14234–14241 (2019).
50. Veisi, H. *et al.* Copper nanoparticle anchored biguanidine modified Zr-UiO-66 MOFs: A competent heterogeneous and reusable nanocatalyst in Buchwald-Hartwig and Ullmann type coupling reactions. *RSC Adv.* **11**, 22278 (2021).
51. Lazaro, I. A., Wells, C. J. R. & Forgan, R. S. Multivariate modulation of the Zr MOF UiO-66 for defect-controlled combination anticancer drug delivery. *Angew. Chem. Int. Ed.* **59**, 5211–5217 (2020).
52. Fortea-Pérez, F. R. *et al.* Sustainable carbon–carbon bond formation catalyzed by new oxamate-containing palladium(II) complexes in ionic liquids. *J. Organomet. Chem.* **743**, 102–108 (2013).
53. Liu, Q. X. *et al.* NHC Pd^{II} complex bearing 1,6-hexylene linker: Synthesis and catalytic activity in the Suzuki–Miyaura and Heck–Mizoroki reactions. *Eur. J. Org. Chem.* **2013**, 1253–1261 (2013).
54. Ghiaci, M., Zargani, M., Moeinpour, F. & Khojastehnezhad, A. Preparation, characterization and application of silica-supported palladium complex as a new and heterogeneous catalyst for Suzuki and Sonogashira reactions. *Appl. Organometal. Chem.* **28**, 589–594 (2014).
55. de Paula, V. I., Sato, C. A. & Buffon, R. Pd complexes based on phosphine-linked cyclophosphazenes: Synthesis, characterization and application in Suzuki coupling reactions. *J. Braz. Chem. Soc.* **23**, 258 (2012).
56. Shakil Hussain, S. M. *et al.* Palladium–bis (oxazoline) complexes with inherent chirality: Synthesis, crystal structures and applications in Suzuki Heck and Sonogashira coupling reactions. *Polyhedron* **70**, 39–46 (2014).
57. Sobhani, S., Ghasemzadeh, M. S., Honarmand, M. & Zarifi, F. Acetamidine–palladium complex immobilized on γ-Fe_2O_3 nanoparticles: a novel magnetically separable catalyst for Heck and Suzuki coupling reactions. *RSC Adv.* **4**, 44166–44174 (2014).
58. Sobhani, S. & Zarifi, F. Pd-isatin Schiff base complex immobilized on γ-Fe_2O_3 as a magnetically recyclable catalyst for the Heck and Suzuki cross-coupling reactions. *Chin. J. Catal.* **36**, 555–563 (2015).

Acknowledgements

We are thankful to Payame Noor University (PNU), Tehran, Iran for financial supports and Gobardanga Hindu College for providing research facilities.

Author contributions

H.V.: Idea generator, Conceptualization, Supervision, Project management. M.A., S.A.K. and S.G.S.: Experimental. T.T.: Original draft writing, Data analysis, M.P. and M.N.: Experimental, Data analysis. B.K.: Original draft writing, Data analysis, Writing—review & editing.

Competing interests

The authors declare no competing interests.

Additional information

Correspondence and requests for materials should be addressed to H.V., T.T. or B.K.

Reprints and permissions information is available at www.nature.com/reprints.